Clinical Hemorheology and Microcirculation 61 (2015) 259–277
DOI 10.3233/CH-151998
IOS Press

Shell matters: Magnetic targeting of SPIONs and *in vitro* effects on endothelial and monocytic cell function

Jasmin Matuszak[a], Philipp Dörfler[a], Jan Zaloga[a], Harald Unterweger[a], Stefan Lyer[a], Barbara Dietel[b], Christoph Alexiou[a] and Iwona Cicha[a,*]

[a]*Section of Experimental Oncology und Nanomedicine (SEON), ENT-Department, Erlangen, Germany*
[b]*Laboratory of Molecular Cardiology, Department of Cardiology and Angiology, University Hospital Erlangen, Germany*

Abstract.
Superparamagnetic iron oxide nanoparticles (SPIONs) are versatile and easily functionalized agents with high potential for diagnostic and therapeutic intravascular applications. In this study, we analyzed the responses of endothelial (ECs) and monocytic cells to three different types of SPIONs, in order to assess the influence of physico-chemical properties on the biological reactions to SPIONs. The following formulations were used: (1) Lauric acid-coated and BSA-stabilized SPION-1,(2) Lauric acid/BSA-coated SPION-2 and (3) dextran-coated SPION-3. SPION-1 were strongly internalized by ECs and reduced their viability in static conditions. Additionally, they had a dose-dependent inhibitory effect on monocytic cell chemotaxis to MCP-1, but did not affect monocytic cell recruitment by ECs. SPION-2 uptake was less pronounced, both in ECs and monocytic cells, and these particles were better tolerated by the vascular cells. Not being internalized by endothelial or monocytic cells, SPION-3 did not induce relevant effects on cell viability, motility or endothelial-monocytic cell interactions.

Taken together, localized accumulation of circulating SPION under physiologic-like flow conditions and their cellular uptake depends on the physicochemical characteristics. Our findings suggest that SPION-2 are suitable for magnetic targeting of atherosclerotic plaques. Due to their excellent biocompatibility and low internalization, SPION-3 may represent a suitable imaging agent for intravascular applications.

Keywords: Atherosclerosis, magnetic nanoparticles, SPION uptake, endothelial-monocytic cell interactions, endothelial migration, monocytic cell chemotaxis, live-cell analysis

1. Introduction

Superparamagnetic iron oxide nanoparticles (SPIONs) and ultra-small superparamagnetic iron oxide nanoparticles (USPIOs) are used for many diagnostic applications, such as magnetic resonance imaging (MRI) of lymph nodes, liver, intestines, and the cardiovascular system. SPION/USPIOs consist of an iron oxide core, often coated with a shell of organic materials such as fatty acids, polysaccharides, or polymers [18, 38]. Coating stabilizes the particles and allows their functionalization with affinity ligands, radiotracers or fluorochromes, offering the possibility of multimodal imaging of intracellular targets.

*Corresponding author: Iwona Cicha, PhD, Cardiovascular Nanomedicine Unit, Section of Experimental Oncology and Nanomedicine, ENT Department, University Hospital Erlangen, Glückstr. 10a, 91054 Erlangen, Germany. Tel.: +49 9131 8543953; Fax: +49 9131 8534282; E-mails: Iwona.Cicha@yahoo.com; Iwona.Cicha@uk-erlangen.de

SPION/USPIO potential for molecular imaging constitutes one of their advantages over contrast-enhanced ultrasound,which is used diagnostically in the same diseases [9, 33, 45]. Moreover, as the magnetic properties of SPIONs allow the remote control of their accumulation by means of an external magnetic field [20, 34, 44], their use for experimental therapeutic applications (drug delivery, and hyperthermia) continues to increase [4, 18]. These physical properties together with their low cytotoxicity [15] appear to warrant a broad usage of SPION/USPIOs in biomedicine.

In cardiovascular imaging, USPIO-based contrast agent ferumoxtran (Sinerem)was extensively utilized as a tool to detect and characterize atherosclerotic plaques, based on the specific incorporation of USPIO by activated macrophages (reviewed in [32]). The ability of USPIO-enhanced MRI to identify plaque inflammation and vulnerability was confirmed in multiple studies [17, 35, 36]. USPIO-enhanced MRI was also shown capable of identifying inflammation within otherwise morphologically "stable" plaques [14], and of detecting inflammatory activity in asymptomatic patients [30, 31]. The feasibility of longitudinal sequential USPIO-enhanced MR imaging at 0, 6, and 12 months was investigated in patients with a moderate asymptomatic carotid stenosis [25]. Apart from important information on quantitative reproducibility of the technique, this study provided evidence that within the 6 months, USPIO nanoparticles were cleared out of the atherosclerotic plaque. Importantly, no major adverse effects following multiple infusions were observed [25], indicating that the UPIO-based contrast agent is clinically safe.

Other clinical studies demonstrated the ability of USPIO-enhanced MRI to predict the expansion and rupture of life-threatening aortic aneurysms [23], to detect inflammation following the ischaemic stroke [26, 27] and to characterize the myocardial infarct pathology [2, 40, 41]. In the latter studies, a strong accumulation of USPIO (ferumoxytol, Rienso) in the infarct tissue allowed a better characterization of the injured myocardium and inflammatory macrophage accumulation, as well as the extent and composition of the peri-infarct zone, as compared with Magnevist® [40].

Apart from providing prognostic information and aiding disease diagnosis, SPION/USPIO can constitute a useful tool both for monitoring the treatment efficacy [29] and for the assessment of future event risk in asymptomatic patients with carotid atherosclerosis [10]. Moreover, SPION-labeling enables visualization of the cells *in vivo* for the purpose of monitoring of cell therapies and tracking inflammatory cells by MRI [24]). In terms of disease treatment, a novel experimental method to overcome the disadvantages of systemic pharmacological therapies is magnetic drug targeting [20, 34, 44]. By loading SPIONs with antiatherosclerotic/antiinflammatory drugs and their magnetic accumulation at the site of atherosclerotic lesion, the efficacy of pharmacological agents could be dramatically increased, contributing to the improved outcomes [7, 8].

In spite of the promising results of the pilot studies in humans, the marketing of iron oxide-containing agents is at the still-stand. Although many SPION and USPIO have been approved for clinical use in the past, currently they are scarcely available, with the exception of the oral iron oxide contrast agent, ferumoxsil (Lumirem), and ferumoxytol (Rienso), an intravenous agent approved for iron replacement therapy in chronic renal failure patients with iron-deficiency anemia. SPION/USPIO had been reported to have favourable safety profiles [5], but the delayed toxicity effects due to an increased oxidative stress could not be entirely excluded [39]. Recent clinical studies indicate that a new generation of SPION formulations can represent a versatile and easily functionalized platform for the development of theranostics with superior clinical and prognostic value [22]. Thus, our aim is to develop effective and safe SPIONs for the diagnosis and therapy of clinically relevant atherosclerosis. For this purpose, extensive analyses of the SPION effects on the vascular cell functions are necessary in order to predict *in vivo* responses. As the cellular effects of different SPIONs may differ depending on their size, charge, and coating [3], we investigated the endothelial and monocytic cell responses to different SPION formulations.

2. Materials and methods

2.1. Materials

Cell culture reagents and media were obtained from Promo Cell (Heidelberg, Germany). Accutase™ was from PAA Laboratories (Linz, Austria) and dispase from Life Technologies GmbH (Darmstadt, Germany). Monocyte chemotactic protein-1 (MCP-1) was purchased from Peprotech (Hamburg, Germany).

Bovine serum albumin (BSA) and iron (II) chloride tetrahydrate were from Merck, Darmstadt, Germany. Lauric acid, epichlorohydrin, dextranT6 (Mw = 6 kDa) and iron (III) chloride hexahydrate were from Sigma Aldrich, Munich, Germany. NaOH, HCl (25%), NH3 (25%), and nitric acid (65%w/w) were from Roth. All compounds used were of pharmaceutical (Ph. Eur) or highly pure (≥99%) grade and were used without any further purification.

2.2. Nanoparticles

The three tested types of SPIONs were synthesized at the Section of Experimental Oncology and Nanomedicine, University Hospital Erlangen. SPION-1: Lauric acid-coated iron oxide nanoparticles were synthesized using a coprecipitation method as described by Tietze et al. [34]. Briefly, Fe (II) and Fe (III) salts at a defined molar ratio (Fe3+/Fe2+ = 3:2) were dissolved in water, followed by addition of NH_3 solution under stirring. The precipitate was then washed with 1.3% ammonium hydroxide solution, followed by the addition of lauric acid and heating to 90°C for 4 min under stirring [16]. The resulting lauric acid-coated particles were washed 10 times with 1.3% ammonium hydroxide solution. Prior to their use in cell culture studies, the SPION-1 were stabilized by incubation 1:1 with a freshly prepared 10% bovine serum albumin (BSA) solution (Merck, 1.12018) and sterilized by filtration through a 0.22 μm filter (Roth, Germany).

SPION-2: Lauric acid/BSA-coated iron oxide nanoparticles were synthesized by coprecipitation, subsequent in situ coating with lauric acid, and formation of an artificial albumin corona as described by Zaloga et al. [42]. Briefly, Fe (II) and Fe (III) salts at a defined molar ratio (Fe3+/Fe2+ = 2) were dissolved in 20 mL of water and stirred at 80°C under argon atmosphere, followed by addition of 20 mL of NH3 solution (25%). The solution was heated to 90°C and 1.25 g lauric acid, dissolved in acetone, was added. The brownish suspension was left to homogenate for 30 min at 90°C. The suspension was then dialyzed multiple times against ultrapure water. Subsequently, SPIONs were stabilized by incubation with a freshly prepared 20% BSA solution, purified by centrifugal ultrafiltration (molecular weight cut-off 100 kDa), and sterilized by filtration through a 0.22 μm filter.

SPION-3: For the preparation of dextran-coated iron oxide nanoparticles, the synthesis method described by Unterweger et al. was used [37]. Briefly, Fe (II) and Fe (III) salts in molar ratios (Fe3+/Fe2+ = 2) as well as 1.75 g of dextran T6 were dissolved in water. After cooling to 4°C under continuous stirring and argon atmosphere, 5 mL of ice-cold 25% NH3 was added. After 5 min, the reaction mixture was heated and kept at 75°C for a further 40 min, followed by cooling to RT and dialysis (molecular weight cut-off 8 kDa). The mixture was then cleared from excess dextran and concentrated to a total volume of 20 mL using ultrafiltration (molecular weight cut-off 100 kDa). To stabilize the dextran coating, crosslinking was performed by adding 4 mL of epichlorohydrine dropwise to the nanoparticle suspension after alkalization with NaOH under vigorous stirring for 24 h. The solution was then dialyzed against water, concentrated by ultrafiltration and sterile filtered through 0.22μm membrane.

2.3. Nanoparticle characterization

For nanoparticle characterization, hydrodynamic diameter and ζ potential of SPIONs were measured as previously reported [21, 37, 42]. Measurements of size were performed in triplicate using Nanophox (Sympatec, Clausthal-Zellerfeld, Germany) on the SPION suspension diluted to an iron concentration of 25 μg/mL with distilled water. ζ potential of SPIONs in distilled water or cell culture medium was measured with a NICOMP 380ZLS (Nicomp, Port Richey, FL, USA) at an iron concentration of 25 μg/mL. Transmission electron microscopy (TEM) pictures were taken with a CM 300 UltraTWIN (Philips, Eindhoven, Netherlands) operated at an acceleration voltage of 300 kV. Samples were prepared by drying 10 μL of diluted nanoparticle suspension on a carbon-coated copper grid (Plano, Wetzlar, Germany).

2.4. Cell culture

Human umbilical vein endothelial cells (HUVECs) were isolated from freshly collected umbilical cords (kindly provided by the Dept. of Gynaecology, Prof. Beckmann, University Hospital Erlangen) using an established technique [6]. The use of human material was approved by the local ethics committee at the University Hospital Erlangen (review No. 4449). Cells were cultured in Endothelial Cell Growth Medium (ECGM, PromoCell, Heidelberg, Germany) with endothelial cell growth supplement containing 5% foetal calf serum, 4 μL/mL heparin, 10 ng/mL epidermal growth factor, 1 μg/mL hydrocortisone, 50 μg/mL gentamycin sulphate, and 50 ng/mL amphotericin B, at humidified 5% CO_2 atmosphere. In all experiments, HUVECs at passage 1-2 were used.

THP-1 monocytic cells were cultured in RPMI 1640 medium supplemented with 2 mmol/L glutamine, 100 U/mL penicillin, 100 μg/mL streptomycin and 10% fetal calf serum. Viability of cells was greater than 98% as estimated by Trypan blue exclusion.

2.5. Live-cell microscopy

HUVECs were seeded in 96-well plates at 2×10^3 cells/well in 100 μL medium. At 24 h after seeding, additional 100 μL of media containing different concentrations of nanoparticles were added to the wells as follows: (a) for controls, 100 μL of pure medium without nanoparticles, and (b) for the treatment samples, 100 μL of medium containing nanoparticles at concentrations 2x higher than the required final nanoparticle concentration. The final SPION concentrations, calculated as total iron (Fe) concentration,were as follows: 0, 25, 50, 100 μg/mL. Cell growth was monitored for 72 h using a live cell-imager (IncuCyte FLR microscope system, Essen Bioscience, AnnArbor, USA) placed in a humidified incubator at 37°C and 5% CO_2. The experiments were performed in hexaplicate.

2.6. Real-time cell analysis

The xCELLigence system (RTCA DP Analyzer, ACEA Bioscience. San Diego, USA) was used for monitoring the effects of nanoparticles on HUVEC viability [21]. The system was placed in a humidified incubator at 37°C and 5% CO_2. Experiments were performed in 16-well E-plates (ACEA Bioscience, San Diego, USA), in which the impedance is measured with the help of microelectrodes localized at the bottom of the wells. This technique calculates a dimensionless parameter called cell index, derived from a relative change in the measured electrical impedance, which is a function of cell viability, number,

morphology, and adhesion strength. Briefly, when cells are not present or do not adhere to the electrodes, the cell index is zero. The presence of cells attached to the electrodes affects the local ionic environment at the electrode/solution interface, leading to an increase in the electrode impedance displayed as cell index values. The higher the number of cells attached on the electrodes, the larger the cell index. Thus, cell index is a quantitative measure of adherent cell number present in each well. Additionally, the quality of the cell interaction with the electrodes (e.g. increased cell adhesion or spreading) will lead to a larger change in electrode impedance. Therefore, changes in cell status, such as cell morphology, strength of adhesion, or cell viability lead to a change in cell index.

For the background measurement, 100 μL of cell-free endothelial cell growth medium was added to the wells. Afterwards, 50 μL of media from each well were replaced with 50 μL of cell suspension containing 2×10^3 HUVECs. About 30 min after seeding of the cells, monitoring of impedance by the xCELLigence system was initiated. At 24 h after seeding, an additional 100 μL of media containing different concentrations of nanoparticles were added to the wells, as described in detail above. Cell growth was monitored every 10 min for 96 h. The experiments were performed in hexaplicate.

2.7. Flow experiments

The bifurcating flow-through cell culture slides were obtained from Ibidi® (Munich, Germany). Numerical flow simulation [6] distinguished the region of laminar shear stress (10.2–10.8 dyne/cm^2 at a flow rate of 9.6 mL/min) throughout the straight main channel, and the region of non-uniform shear stress at the outer walls of bifurcation (shear stress range from ∼6.3 dyne/cm^2 to ∼0.5 dyne/cm^2).

To test the effects of circulating SPIONs on endothelial viability, HUVECs at 7×10^5/mL were seeded in the bifurcating slides and grown until confluence. Using a programmed peristaltic pump (Ismatec, Wertheim, Germany), the cell monolayer inside the slide channel was perfused with medium (with 0–100 μg/mL SPIONs) at arterial shear stress (10 dyne/cm^2, corresponding to flow rate of 9.6 mL/min) for 18 h. After 18 h, slides were detached from the pump system, washed with PBS and fixed with 4% formalin for 10 min at RT. HUVECs were stained with Alexa488-phalloidin (PromoKine, Heidelberg, Germany). Cell nuclei were counterstained with DAPI (Molecular Probes, Darmstadt, Germany).

2.8. Magnetic accumulation of nanoparticles

To investigate the magnetic accumulation of circulating SPIONs, a magnet was positioned directly at the outer wall of the bifurcation (Supplementary Figure 1A). Two different concentrations of SPIONs were used (3 μg/mL and 30 μg/mL). Subsequently, particles were stained with Prussian blue (1:1 potassium ferrocyanide (2%) and hydrochloric acid (2%)) for 30 min at RT to assess the uptake of circulating SPIONs. Nuclei of the cells were counterstained with nuclear fast-red (Merck) for 10 min at RT, followed by rinsing with distilled water and repeated washing with 100% of ethanol. As a mounting medium, Mowiol (Roth, Karlsruhe, Germany) was added to extend staining durability.

2.9. Adhesion molecule expression

To investigate the effects of SPIONs accumulation (3 μg/mL with magnet or 30 μg/mL without magnet) on the TNF-α-induced adhesion molecule expression at bifurcations, HUVECs were stained with primary antibody against E-Selectin (Clone BBIG-E4, R&D Systems,Wiesbaden, Germany) and VCAM-1 (Clone BBIG-V1, R&DSystems) as described before [6]. Adhesion molecule expression was analysed using

fluorescence microscope Zeiss Axio Observer. Z1 (Carl Zeiss AG, Oberkochen, Germany)and ImageJ software.

2.10. Monocyte adhesion assay

Following the exposure to flow with or without magnetic accumulation of SPIONs and stimulation with TNF-α, cells in bifurcating slides were perfused for 1 h with fresh endothelial cell medium containing THP-1 monocytic cells (7×10^5 cells/mL). Non-adherent cells were removed by stringent washing. Following the fixation with 4% paraformaldehyde, adherent monocytic cells were visualized using hematoxylin-eosin stain (Dako, Hamburg, Germany) and digitally counted in minimum 8 image fields (0.89 mm^2) at x100 magnification in non-uniform shear stress area.

2.11. Endothelial cell migration assay

HUVEC migration was assessed in a modified barrier assay using silicone cell culture inserts from Ibidi (Munich, Germany). HUVECs were seeded in 2 wells separated by a 500 μm barrier, at a concentration of 3×10^5/mL. The cells were treated with 0, 50 and100 μg/mLSPIONs overnight. Following the removal of inserts, HUVECs were washed and incubated with medium for up to 24 h. The gap between the 2 monolayers was recorded at the insert removal point (0 h), at 12 and 24 hours using an Incucyte FLR system. Cell-free areas at different time points were measured using ImageJ software. The effect of SPION-preincubation on cell migration was assessed by calculating the increase in the area occupied by cells at later time points compared with the cell-covered area at 0 h.

2.12. Chemotaxis assay

The effect of SPIONs (0–100 μg/mL, 2 h) on monocytic cell migration was assessed in a 96-well Chemo-Tx plate (NeuroProbe, Gaithersburg, MD, USA). THP-1 monocytic cells were incubated with 0, 12.5, 25, 50 or 100 μg/ml particles for 2 h at 37°C and under constant stirring. Briefly, the microplate wells were filled with 30 μL serum-free RPMI 1640. MCP-1 (50 ng/mL) was used as a positive control. After placing the filter frame, the filter top sites with 5 μm-pores were filled with 25 μL of nanoparticle-treated monocytic cells at a concentration of 1×10^6 cells/mL. Following incubation for 1 h at 37°C, migrated non-adherent cells from the lower wells were fixed and counted using flow cytometry. All samples were run in quadriplicate and averaged. The mean number of migrated cells in the negative control (MCP-1 unstimulated) samples was set as 1.

2.13. Flow cytometry

Flow cytometry (Gallios, Beckman Coulter, Fullerton, USA) was employed to investigate uptake of SPIONs by endothelial cells and THP-1. For the analysis of uptake by endothelial cells, HUVECs were seeded in 24-well plates and grown overnight. Subsequently, the culture medium was replaced by medium supplemented with SPIONs at 3 and 30 μg/mL. After 24 h cells were washed with PBS, harvested and stained with nuclear dye Hoechst 33342 (Life Technologies) to discriminate between cells and nanoparticles. The side scatter, which increases with particle uptake [12] was measured in all Hoechst-positive events. To analyse the SPION uptake by THP-1 monocytic cells during the chemotaxis assays, 2×10^6/mL cells were treated with medium supplemented with SPION at 12.5–100 μg/mL for 2 h.

Subsequently, 50 μL of the cell suspension was used for counting the THP-1 cell numbers with the help of flow-count fluorospheres (Beckman Coulter) and measuring the side scatter. Electronic compensation was used to eliminate bleed through fluorescence.

2.14. Quantification of iron load per cell

The iron concentration per cell was quantified with microwave plasma atomic emission spectroscopy (MP-AES, 4200 device, Agilent). HUVECs seeded at a density of 0.1×10^6 cells in a 25 cm^2 cell culture flask were grown until 80% confluence. Cells were then incubated with SPION-containing medium for 24 h, followed by harvesting, washing with medium and counting. After centrifugation, cell pellets containing specified number of cells were dissolved in nitric acid for 15 min at 95°C and 1000 rpm. After addition of 450 μL of water the emission spectrum of the samples was analysed and compared to the standard curves.

2.15. Statistical analyses

The SigmaPlot® Software was used for statistical analyses. Data are expressed as mean ± SEM, unless stated otherwise. The comparison between untreated and SPION-treated samples was done using Signed Rank test of paired Student's *T*-test. $P < 0.05$ was considered statistically significant.

3. Results

3.1. Long-term effect of SPIONs on EC viability in static and dynamic conditions

In the present study, the SPION formulations with the following characteristics were used: SPION-1 with 126 nm hydrodynamic diameter and ζ-potential of –34.6 mV, SPION-2 with 79 nm hydrodynamic diameter and ζ-potential of –37.3 mV, and SPION-3 with 78 nm hydrodynamic diameter and ζ-potential of +0.1 mV (Supplementary Figure 1B). The effects of these SPION formulations on endothelial viability were first investigated in static cell culture conditions using real-time cell analysis. The cell index measured with this technique increased steadily over time in control (untreated) endothelial cells.Upon treatment with SPION-1 (0–100 μg/mL) a progressive dose-dependent decrease in cell viability and was observed with the treatment time (Fig. 1A, upper panel). At 24 h post-application, cell index relative of the control samples was reduced by 50% in HUVECs treated with 100 μg/ml SPION-1.

SPION-2 were better tolerated over 72 h of treatment. In cells treated with 50 μg/mL SPION-2 (Fig. 1B), a decrease in cell index was observed first at 48 and 72 h in comparison to control, indicative of cell growth inhibition or loss of adherence. At the concentration of 100 μg/mL SPION-2, the decrease in endothelial cell index relative to pre-application values was observed (indicative of negative effects on cell viability or adherence was induced) (Fig. 1B). In the cells treated with SPION-3, an increase of cell index similar to control samples was observed at all concentrations, until the end of the measurement at 72 h post-application (Fig. 1C). The application of SPIONs alone (without cells) had no effect on the impedance measurements, with cell index values in the presence of SPIONs oscillating between 0 and –0.1 for all SPION formulations.

The above findings were confirmed using live cell microscopy in parallel samples, which allowed the observation of cell morphology and the measurement of confluence. Using this method, however,

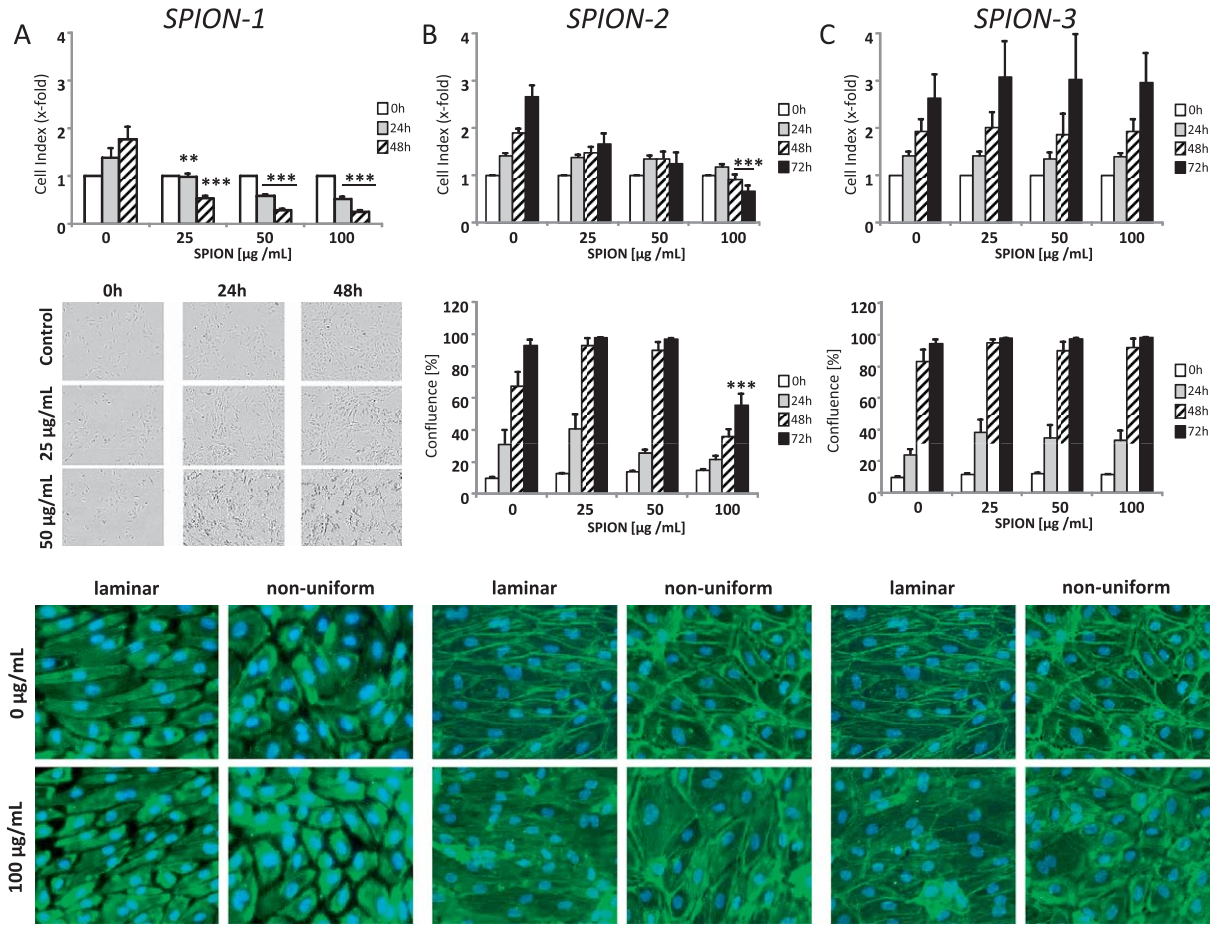

Fig. 1. Effects of SPIONs on endothelial cell viability.SPION-1 (A), SPION-2 (B) and SPION-3 (C) are shown. Upper panel:Real-time cell analyzer measurements in static conditions; Cell index values obtained in untreated control samples at 0 h were set to 1. Middle panel: Live-cell imaging of SPION-treated HUVECs (static conditions); Original images are shown for SPION-1 (left) and confluence quantification for SPION-2 and SPION-3. Lower panel: HUVECs morphology upon the exposure to circulating SPIONs (0 and 100µg/mL; 18 h) visualized with phalloidin (green, cytoskeleton) and Hoechst (blue, nucleus) staining. Images were taken at 20× objective magnification. Values obtained in untreated control samples were set to 1. Data are expressed as mean ± SEM; $n = 3$. $^{**}p < 0.01$; $^{***}p < 0.001$ vs. control. Signed Rank test of paired Student's *T*-test.

proved challenging in samples treated with SPION-1 as the particles disturbed imaging. To overcome this problem, the wells treated with SPION-1 were washed prior to the scans after 24 h and 48 h. This procedure enabled microscopic imaging, but did not allow correct measurements of confluence by the live-imaging system, so that no confluence quantification is shown for SPION-1 in Fig. 1A. Decreased cell numbers were observed upon 24 h treatment with 25µg/mL SPION-1 and with 100 µg/mL SPION-2 for 72 h. In contrast, SPION-3 were well tolerated by endothelial cells and did not affect the morphology or confluence of cells as compared with controls (Fig. 1C, middle panel).

As nanoparticle sedimentation in static cell culture conditions increases the effective concentrations of SPIONs on the adherent cells, we additionally investigated whether the same concentrations of circulating SPIONs affect endothelial viability. Under physiologic-like flow conditions, the endothelial cells exposed to the three types of SPIONs at 100 µg/mL for 18 h remained viable, without any dramatic alterations in

morphology (Fig. 1A-C, lower panel) and their resistance to shear stress was unchanged, as indicated by the lack of cellular detachment.

3.2. Effects of different SPION formulations on cell migration

Endothelial cell migration was assessed utilizing a modified wound-closing assay. In the cells pre-incubated overnight with SPIONs up to 50 μg/mL, no significant effect on migration speed was observed as compared to control untreated cells (Fig. 2A-C). Consequently, no differences in migration between ECs treated with the different SPION types were detected.

In the case of THP-1 monocytic cell chemotaxis, differential effects of the SPION formulations (0–100 μg/mL) were observed. Whereas the incubation with dextran-coated SPION-3 did not affect the THP-1 chemotaxis in response to MCP-1, in SPION-1 treated cells, a dose-dependent decrease in chemotactic response was observed (Fig. 3). This decrease occurred in parallel with the increase in cell granularity as measured by side-scatter, indicating an enhanced uptake of the SPION-1 by monocytic cells. At 100 μg/mL SPION-1, a 25% increase in side scatter relative of untreated control was detected. Interestingly, upon the treatment with SPION-2,40% decrease in the monocytic cell chemotaxis was observed as compared with positive control, but this decrease was not dose-dependent (Fig. 3). As indicated by the side scatter measurement, SPION-2 were less avidly internalized by THP-1 monocytic cells, with 10% increase in cell granularity at 100 μg/mL of SPION-2 as compared to untreated controls (Fig. 3B). Within 2 h of incubation, no effect of SPION treatment on monocytic cell viability was detected (Supplementary Figure 2).

3.3. Magnetic accumulation of circulating SPIONs

Magnetic drug targeting offers a promising alternative to systemic administration of cardiovascular agents. In order to investigate the possibility of accumulating the circulating SPIONs by an external magnetic force, a magnet was placed at the outer wall of bifurcation as described in our initial studies [21]. Following the perfusion with SPIONs for 18 h, the accumulated nanoparticles were visualized using Prussian blue stain. In the absence of magnetic field, no region-specific accumulation was observed for

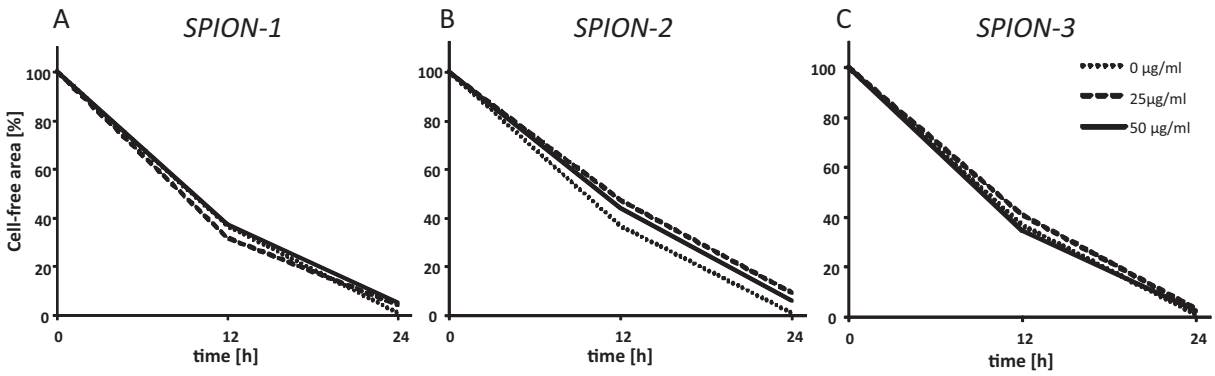

Fig. 2. Effect of SPIONs on endothelial cell migration. HUVECs were pre-treated with 0, 50 and 100 μg/mL SPION-1 (A), SPION-2 (B) and SPION-3 for 24 h. A gap between two cell layers was created using a cell culture insert. After removal of the insert, cell migration was monitored for 24 h. Analysis was performed with ImageJ. Data are expressed as mean ± SEM; $n = 3$.

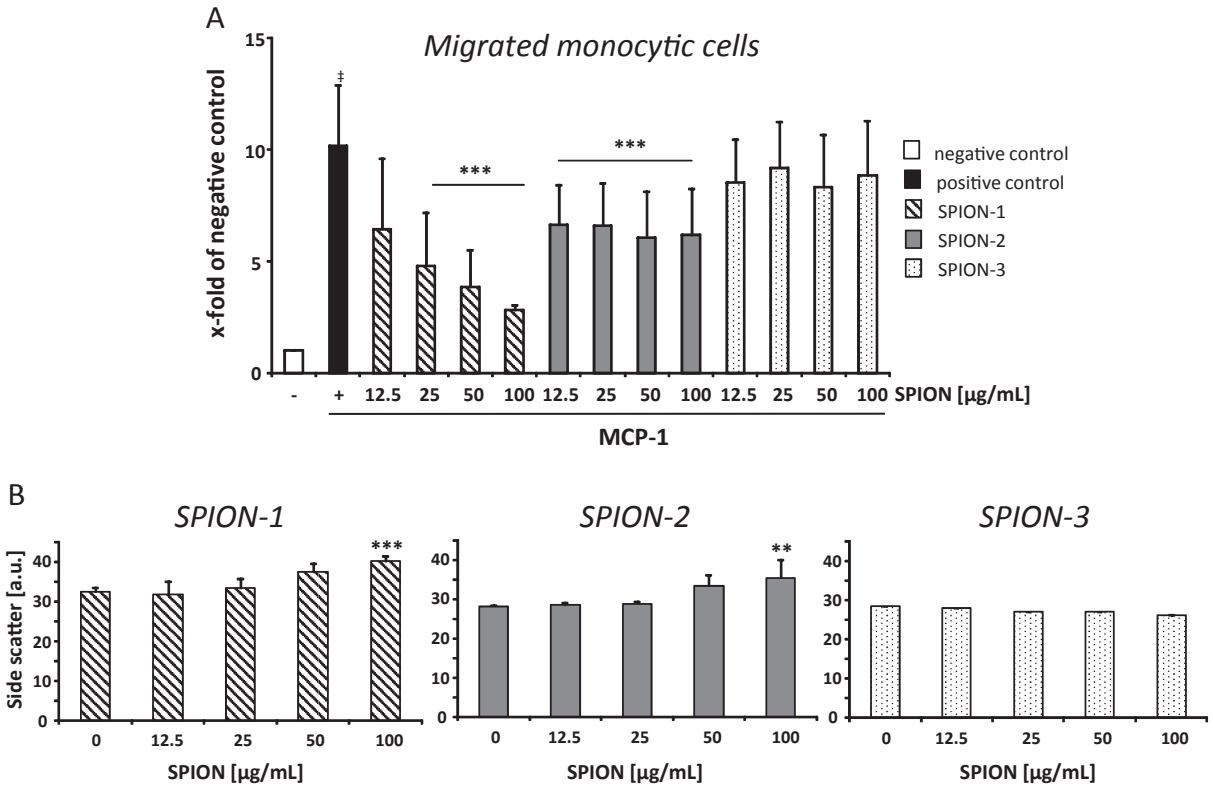

Fig. 3. Monocytic cell chemotaxis and SPION uptake. (A) THP-1 chemotaxis towards MCP-1 after treatment with SPION-1 (red), SPION-2 (blue) and SPION-3 (green) for 2 h. Shown is the x-fold of negative control (without MCP-1). (B) The side scatter in THP-1 monocytic cells measured with flow cytometry is shown. Data are expressed as mean ± SEM; $n = 4$. $^{**}p < 0.01$; $^{***}p < 0.001$ vs. control. $^{‡}p < 0.001$. Signed Rank test of paired Student's *T*-test.

any of the tested SPIONs (30 μg/mL), albeit an overall increased accumulation of iron was detected in the endothelial cells treated with SPION-1 as compared with SPION-2 and SPION-3. We have therefore investigated the possibility of enhancing the SPION accumulation, in parallel reducing the circulating dose of the particles 10 times, down to 3 μg/mL. As shown in the Fig. 4, upon the magnetic field application, the accumulation of large amounts of SPION-1 was observed at the outer wall of bifurcations. In contrast, smaller amounts of circulating SPION-2 were accumulated in the region of interest under external magnetic field, and no accumulation or localized uptake of SPION-3 was detectable using Prussian blue stain (Fig. 4).

3.4. Effects of SPIONs on monocytic cell recruitment under flow

In order to investigate the effect of accumulated SPIONs on the endothelial-monocytic cell interactions and adhesion molecule expression in response to TNF-alpha, HUVECs were perfused with 30 μg/mL SPIONs in the absence of external magnet or with 3 μg/mL in the presence of magnetic field. Subsequently, the cells were treated with TNF-alpha for 2 h, followed by the dynamic adhesion assay or the analysis of adhesion molecule expression. Overall, no major effects of SPIONs on the TNF-alpha induced monocytic

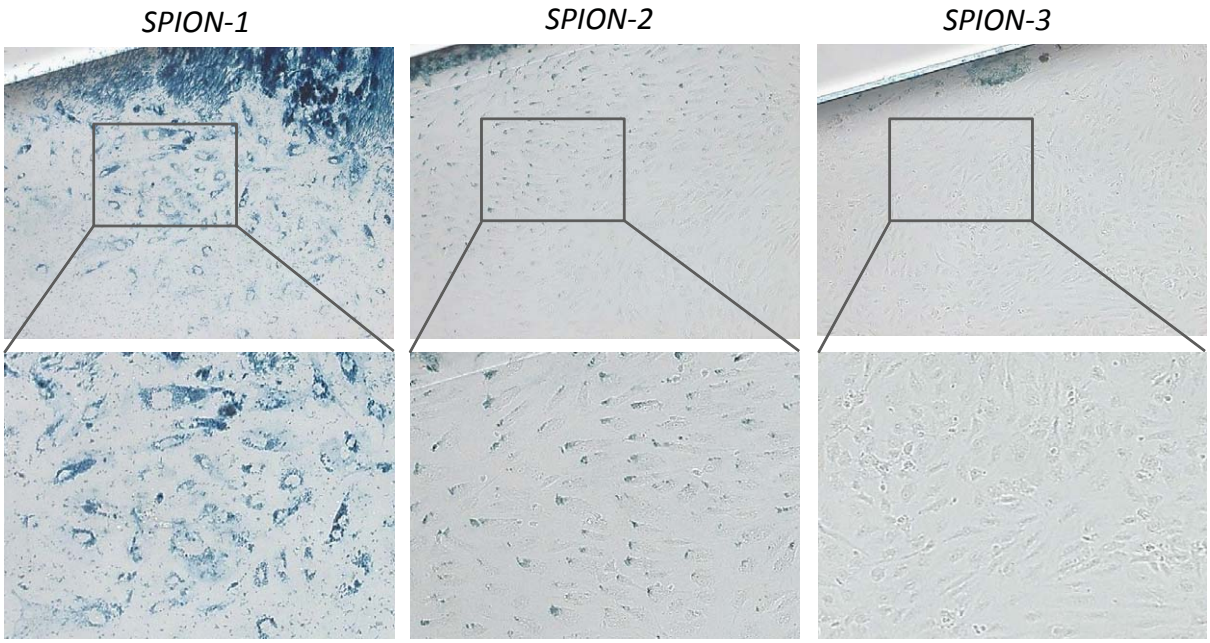

Fig. 4. Magnetic accumulation of circulating SPIONs at the non-uniform shear stress region. HUVECs in bifurcating flow-through slides were perfused with 3 μg/mL SPION-1, SPION-2 and SPION-3 (18 h; 10 dyne/cm^2), in the presence of an external magnet placed at the outer wall of bifurcation. Particles were stained with a Prussian blue stain and nuclei of the cells were counterstained with nuclear fast-red. Representative images at 10× and 20× objective magnification from $n = 3$ independent experiments are shown.

cell recruitment by endothelial cells were observed (Fig. 5), where by a slight reduction in the numbers of adherent monocytic cells was detected under non-uniform shear stress upon treatment with 3 μg/mL and 30 μg/mL of SPION-3, and a slight increase in adhesion to HUVECs exposed to 30 μg/mL of SPION-2. In accordance with this, SPION-3 did not markedly affect the expression of endothelial adhesion molecules: only a slight decrease in VCAM-1 was noted at both tested concentration and E-selectin decrease at 30 μg/mL (Supplementary Figure 3). Interestingly, the exposure to accumulated SPION-2 (3 μg/mL) resulted in a significant decrease of VCAM-1 and an increased expression of E-selectin (Fig. 5B). These counterbalancing changes, however, did not affect the net number of monocytes adhering to HUVECs treated with 3 μg/mL of SPION-2. Similar, but somewhat less pronounced adhesion molecule expression pattern was observed upon treatment with SPION-1 (Supplementary Figure 3).

In accordance with the data on particle accumulation by magnetic force, the uptake of SPIONs by HUVECs in the static conditions was strongly dependent on the particle type. As shown in Fig. 6A, a 1.6-fold increase in side scatter values reflecting cell granularity was observed upon incubation of HUVECs with 3 μg/mL of SPION-1 ($p < 0.001$). By increasing the SPION-1 concentration to 30 μg/mL, the side scatter values were further increased (5.3-fold relative of untreated control, $p < 0.001$). Side scatter values, reflecting nanoparticle uptake, were slightly increased in cells treated with SPION-2 at 3 μg/mL (1.1-fold, $p < 0.01$) and 30 μg/mL (1.3 fold, $p < 0.01$). Notably, no increase in side scatter was detectable upon treatment with SPION-3.

To confirm the side scatter measurements, we additionally quantified the iron concentration per cell in SPION-treated HUVECs using MP-AES. The iron load per cell was strongly dependent on the particle

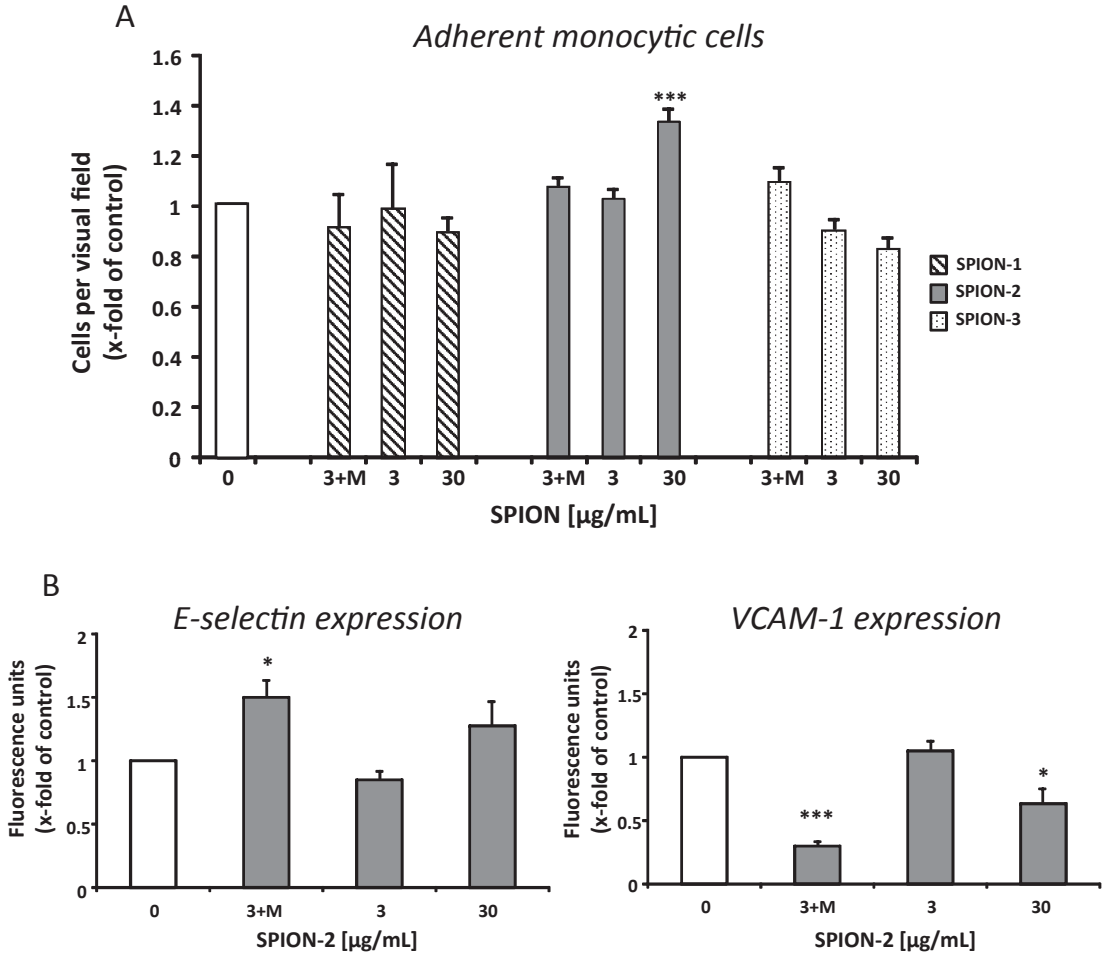

Fig. 5. Effect of accumulated SPIONs on monocytic cell recruitment and endothelial adhesion molecule expression. HUVECs in bifurcation flow through slides were perfused with SPION-1(red), SPION-2 (blue) and SPION-3 (green) for 18 h, followed by stimulation with TNF-α (2 h). SPION concentration are as indicated, where by 3+M denotes the branch with magnet and 3 the branch without magnet. (A) Adherent monocytic cells were quantified after 1 h of dynamic adhesion assay in at least 8 microscopic images per experiment (non-uniform region, 10× objective magnification). (B) SPION-treated HUVECs were stained with primary antibody against E-selectin or VCAM-1 (only SPION-2-treated cells are shown). Fluorescence was quantified in 6–8 microscopic images per experiment (non-uniform region, 20× objective magnification). Values obtained in untreated control samples were set to 1. Data are expressed as mean ± SEM; $n = 3$. $^{*}p < 0.05$; $^{***}p < 0.001$ vs. control. Signed Rank test of paired Student's *T*-test.

type, in accordance with the changes in side scatter. As compared to untreated control, in cells treated with 3 μg/mL SPION-1, a 30-fold increase in iron concentration per cell (0.0015 ng Fe/cell) was observed. At 30 μg/UmL SPION-1, the iron concentration per cell was 600-times larger (0.035 ng Fe/cell) in comparison to the natural iron content in HUVECs (Fig. 6B). The uptake of SPION-2 was less pronounced, resulting in a 2.3-fold increase in iron content at 3 μg /mL (0.00012 ng Fe/cell), and a 8.3-fold increase at 30 μg /mL (0.00042 ng Fe/cell). For SPION-3, no change in iron load per cell in comparison to untreated controls was detectable.

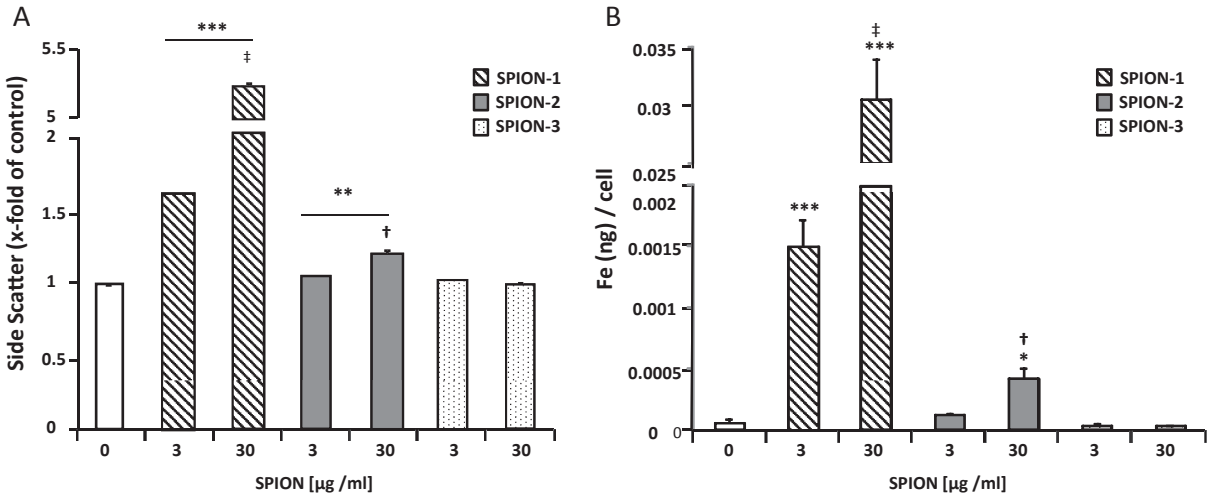

Fig. 6. SPION uptake by HUVECs. HUVECs were incubated in static conditions with 3 and 30 µg/mL SPION-1 (red), SPION-2 (blue) and SPION-3 (green), followed by the analysis of side scatter with flow cytometry (A) and iron load per cell using MP-AES (B). In side scatter analysis,values obtained in untreated control samples were set to 1. Data are expressed as mean ± SEM; $n = 3$. $^{*}p < 0.05$; $^{**}p < 0.01$; $^{***}p < 0.001$ vs. control; $^{\dagger}p < 0.01$; $^{\ddagger}p < 0.001$ vs. 3µg/mL of the same SPION type. Signed Rank test of paired Student's *T*-test.

4. Discussion

Nanosystems designed for the clinical use should correspond to the needs of intended applications: Whereas magnetic drug delivery system should be easily accumulated by external magnetic force and internalized by the target cells, for the imaging nanoparticles, low cellular uptake, bio-inertness and long circulation time are the desirable characteristics. The SPION types used in this study have been previously tested in the pre-clinical MRI either *in vivo* or in silico, showing signal loss in T2 (unpublished data), and their utility for magnetic particle imaging (MPI) is currently under investigation. However, the potential toxicity of SPIONs is an important concern that must be excluded prior to their pilot application in humans [11]. Extensive studies in cell culture models under physiological-like conditions are necessary to predict nanoparticle behaviour *in vivo* [11], including their cellular uptake and the effects on cell signalling and functions. As SPIONs interfere with the available photometric methods for testing cell viability and/or metabolic activity, we have selected several alternative techniques to investigate their effect on endothelial and monocytic cell functions. The studies in static conditions showed that the effects on HUVEC viability were strongly dependent on the SPION type. Whereas SPION-1 affected endothelial cell viability already at 50µg/mL concentration at 24 h of treatment, cells treated for 72 h with up to 100 µg/mL SPION-2 remained viable, and no negative effects of treatment with SPION-3 were detected independent of the concentration or treatment duration. Under flow conditions, all SPION types were equally well tolerated by endothelial cells, indicating that nanoparticle sedimentation in static conditions may increase the effective concentrations of SPION in the vicinity of cell monolayer. In the presence of increased SPION uptake, this may in turn contribute to an enhanced cytotoxicity.

Particle size and surface charge indicated by ζ-potential are some of the critical factors that affect the behaviour of nanoparticles, their cellular uptake, but also stability in biological fluids [1]. Cationic particles are internalized more effectively, likely due to the better affinity to the negatively charged cell

glycocalyx. However, strongly positively charged particles bear the risk of increased hemotoxicity [28]. In our case, the tested SPION types did not dramatically differ in size, nonetheless, the most strongly internalized SPION-1 were markedly larger than the other two types, which might have in part contributed to their enhanced uptake. However, despite the lack of difference in size between SPION-2 and SPION-3, the cellular uptake of these two formulations was significantly different. It has been reported that due to repulsion with the negatively charged cell membrane, particles with a strong negative charge may face reduced cellular uptake [3]. Among the tested formulations, both SPION-1 and SPION-2 had similarly low ζ-potential in water, but they dramatically differed in the amount of cellular uptake. Furthermore, SPION-3, which had no significant surface charge at neutral pH due to the nature of their coating and should not be affected by the charge of the cell membrane, were not internalized by HUVECs at all. This indicates that neither the particle size nor the charge was the key factor influencing their differential cellular uptake. For clinical applications, nanoparticle agglomeration may be a decisive factor limiting their use in patients, as it affects bioavailability, and thus efficacy. Nanoparticles with a ζ-potential above ($\pm$) 30 mV are usually considered as colloidally stable, since the surface charge prevents their aggregation. However, steric repulsion, such as the hindrance provided by a coating of the nanoparticle surface (here, SPION-3 with dextran shell), can also provide high colloidal stability despite a nearly neutral ζ-potential [13]. Comparing the formulations used in our study (SPION-1 with lauric acid shell, SPION-2 with lauric acid/BSA shell and SPION-3 with dextran shell), all types of SPIONs had good colloidal stability in water. However, in the case of SPION-1, the stronger tendency to sediment was observed in the static cell culture conditions. It is therefore plausible that the lauric acid shell contributed to the enhanced aggregation, resulting in increased cellular uptake of SPION-1.The aggregates formed in the cell culture conditions may be taken up even quicker as single particles, as the cellular uptake rate is much higher for particles larger than 100 nm [3]. Additionally, the slight tendency to form aggregates observed in this type of SPIONs may have facilitated their magnetic targeting: As shown in the experiments with circulating nanoparticles, SPION-1 had by far the largest capacity to accumulate at the bifurcation region exposed to the magnetic field.

Interestingly, this enhanced magnetic accumulation of SPION-1 at the outer wall of bifurcation did not significantly affect TNF-α induced monocytic cell recruitment or endothelial activation. Although none of the SPION formulations had a major effect on the numbers of adherent monocytic cells, in the case of SPION-2, a strong inhibition of VCAM-1 expression was observed. As previously shown by Zhang & Frei, albumin selectively inhibits TNF-α-induced expression of VCAM-1 in endothelial cells [43]. It is therefore likely that the suppressive effect of lauric acid/BSA-coated SPION-2 on VCAM-1 induction was associated with the shell composition. This reduction in VCAM-1 expression, however, was counterbalanced by an increased E-selectin level and did not prevent monocytic cell adhesion to a significant extent.

Concerning the effect of SPIONs on the cellular motility, pre-incubation of HUVECs with different SPION formulations did not affect the speed of the spontaneous endothelial cell migration. It must be noted, however, that due to the interference of higher concentrations of SPION-1 with the light microscopy, we were not able to monitor the particle effect on endothelial migration directly during the incubation with SPIONs. Interestingly, SPION-1 had a strong and dose-dependent inhibitory effect on monocytic cell chemotaxis. In parallel with increasing nanoparticle uptake, the chemotaxis to MCP-1 was decreased. Due to a very short incubation time (2 h), the observed effect was likely associated with nanoparticle interactions at the ligand-receptor signalling level rather than affecting de novo protein expression. Further studies will be necessary to investigate the molecular mechanisms of this phenomenon. In the case of SPION-2 treatment, a reduction in monocytic cell chemotaxis was observed as compared to control, but

this effect was independent of the used SPION-2 concentration. Treatment with SPION-3 did not affect the monocytic cell chemotaxis to MCP-1.

It must be noted that the selected concentrations of SPIONs are relevant for the potential biomedical applications: In the animal model, the concentrations of 45–60 μg/mL of blood have been used for magnetic drug targeting purposes [19, 34]. In humans, iron oxide-based contrast agent ferumoxtran is used at a maximal dose of 2.6 mg/kg. Adjusted for the blood volume of 77 mL/kg, this corresponds to the concentration of 33 μg/mL, which is within the range used in our study.

Taken together, our findings indicate that an extensive analysis of cellular responses to SPIONs can facilitate the development of stable nanoparticles with improved biocompatibility. Based on the present results, SPION-2 possess sufficient biocompatibility and suitable magnetic properties to allow their use as carriers for magnetic drug targeting. Furthermore, they can serve for magnetic cell-labeling, being internalized by various cells without inducing major cytotoxicity. In contrast, our studies indicate that SPION-3 constitute a candidate formulation with superb characteristics for imaging purposes. In the next steps, the *in vivo* validation of these particles will be necessary to ensure their safety and efficacy prior to application in humans.

Acknowledgments

This work was supported by the DFG (CI 162/2-1) and the EU ("NanoAthero" project FP7-NMP-2012-LARGE-6-309820). The authors thank Prof. Beckmann (Dept. of Gynaecology, University Hospital Erlangen, Germany) for providing umbilical cords and Eveline Schreiber for preparing SPION-1 and for performing MP-AES measurements. The study was performed in accordance with the Ethical Guidelines for Publication in Clinical Hemorheology and Microcirculation (Clin Hemorheol Microcirc., **44** (2010), 1-2).

References

[1] K.L. Aillon, Y. Xie, N. El-Gendy, C.J. Berkland and M.L. Forrest, Effects of nanomaterial physicochemical properties on *in vivo* toxicity, *Advanced drug delivery reviews* **61** (2009), 457–466.

[2] S.R. Alam, A.S. Shah, J. Richards, N.N. Lang, G. Barnes, N. Joshi, T. MacGillivray, G. McKillop, S. Mirsadraee, J. Payne, K.A. Fox, P. Henriksen, D.E. Newby and S.I. Semple, Ultrasmall superparamagnetic particles of iron oxide in patients with acute myocardial infarction: Early clinical experience, Circulation. *Cardiovascular imaging* **5** (2012), 559–565.

[3] A. Albanese, P.S. Tang and W.C.W. Chan, The effect of nanoparticle size, shape, and surface chemistry on biological systems, *Annu Rev Biomed Eng* **14** (2012), 1–16.

[4] E. Amstad, M. Textor and E. Reimhult, Stabilization and functionalization of iron oxide nanoparticles for biomedical applications, *Nanoscale* **3** (2011), 2819–2843.

[5] H. Bernd, E. De Kerviler, S. Gaillard and B. Bonnemain, Safety and tolerability of ultrasmall superparamagnetic iron oxide contrast agent: Comprehensive analysis of a clinical development program, *Investigative Radiology* **44** (2009), 336–342.

[6] I. Cicha, K. Beronov, E.L. Ramirez, K. Osterode, M. Goppelt-Struebe, D. Raaz, A. Yilmaz, W.G. Daniel and C.D. Garlichs, Shear stress preconditioning modulates endothelial susceptibility to circulating TNF-alpha and monocytic cell recruitment in a simplified model of arterial bifurcations, *Atherosclerosis* **207** (2009), 93–102.

[7] I. Cicha, C.D. Garlichs and C. Alexiou, Cardiovascular therapy through nanotechnology – how far are we still from bedside? *Eur J Nanomed* **6** (2014), 63–87.

[8] I.L. Cicha, S. Lyer, C. Alexiou and C.D. Garlichs, Nanomedicine in diagnostics and therapy of cardiovascular diseases: Beyond atherosclerotic plaque imaging, *Nanotechnology Reviews* **2** (2013), 449–472.

[9] D.A. Clevert, M. D'Anastasi and E.M. Jung, Contrast-enhanced ultrasound and microcirculation: Efficiency through dynamics - current developments, *Clin Hemorheol Micro* **53** (2013), 171–186.

[10] A.J. Degnan, A.J. Patterson, T.Y. Tang, S.P. Howarth and J.H. Gillard, Evaluation of ultrasmall superparamagnetic iron oxide-enhanced MRI of carotid atherosclerosis to assess risk of cerebrovascular and cardiovascular events: Follow-up of the ATHEROMA trial, *Cerebrovascular Diseases* **34** (2012), 169–173.
[11] N. Desai, Challenges in development of nanoparticle-based therapeutics, *The AAPS Journal* **14** (2012), 282–295.
[12] R.P. Friedrich, C. Janko, M. Poettler, P. Tripal, J. Zaloga, I. Cicha, S. Durr, J. Nowak, S. Odenbach, I. Slabu, M. Liebl, L. Trahms, M. Stapf, I. Hilger, S. Lyer and C. Alexiou, Flow cytometry for intracellular SPION quantification: Specificity and sensitivity in comparison with spectroscopic methods, *International Journal of Nanomedicine* **10** (2015), 4185–4201.
[13] S. Hirsjarvi, S. Dufort, J. Gravier, I. Texier, Q. Yan, J. Bibette, L. Sancey, V. Josserand, C. Passirani, J.P. Benoit and J.L. Coll, Influence of size, surface coating and fine chemical composition on the *in vitro* reactivity and *in vivo* biodistribution of lipid nanocapsules versus lipid nanoemulsions in cancer models, Nanomedicine: Nanotechnology, biology, *and medicine* **9** (2013), 375–387.
[14] S.P. Howarth, T.Y. Tang, R. Trivedi, R. Weerakkody, UK-IJ, M.E. Gaunt, J.R. Boyle, Z.Y. Li, S.R. Miller, M.J. Graves and J.H. Gillard, Utility of USPIO-enhanced MR imaging to identify inflammation and the fibrous cap: A comparison of symptomatic and asymptomatic individuals, *European Journal of Radiology* **70** (2009), 555–560.
[15] H.A. Jeng and J. Swanson, Toxicity of metal oxide nanoparticles in mammalian cells, *J Environ Sci Health A Tox Hazard Subst Environ Eng* **41** (2006), 2699–2711.
[16] S.E. Khalafalla and G.W. Reimers, Preparation of dilution-stable aqueous magnetic fluids, *IEEE T Magn* **16** (1980), 178–183.
[17] M.E. Kooi, V.C. Cappendijk, K.B. Cleutjens, A.G. Kessels, P.J. Kitslaar, M. Borgers, P.M. Frederik, M.J. Daemen and J.M. van Engelshoven, Accumulation of ultrasmall superparamagnetic particles of iron oxide in human atherosclerotic plaques can be detected by *in vivo* magnetic resonance imaging, *Circulation* **107** (2003), 2453–2458.
[18] S. Laurent, A.A. Saei, S. Behzadi, A. Panahifar and M. Mahmoudi, Superparamagnetic iron oxide nanoparticles for delivery of therapeutic agents: Opportunities and challenges, *Expert Opin Drug Deliv* **11** (2014), 1449–1470.
[19] S. Lyer, R. Tietze, R. Jurgons, T. Struffert, T. Engelhorn, E. Schreiber, A. Dorfler and C. Alexiou, Visualisation of tumour regression after local chemotherapy with magnetic nanoparticles - a pilot study, *Anticancer Research* **30** (2010), 1553–1557.
[20] Y.H. Ma, S.Y. Wu, T. Wu, Y.J. Chang, M.Y. Hua and J.P. Chen, Magnetically targeted thrombolysis with recombinant tissue plasminogen activator bound to polyacrylic acid-coated nanoparticles, *Biomaterials* **30** (2009), 3343–3351.
[21] J. Matuszak, J. Zaloga, R.P. Friedrich, S. Lyer, J. Nowak, S. Odenbach, C. Alexiou and I. Cicha, Endothelial biocompatibility and accumulation of SPION under flow conditions, *J Magn Magn Mater* **380** (2015), 20–26.
[22] E.A. Neuwelt, B.E. Hamilton, C.G. Varallyay, W.R. Rooney, R.D. Edelman, P.M. Jacobs and S.G. Watnick, Ultrasmall superparamagnetic iron oxides (USPIOs): A future alternative magnetic resonance (MR) contrast agent for patients at risk for nephrogenic systemic fibrosis (NSF)? *Kidney International* **75** (2009), 465–474.
[23] J.M. Richards, S.I. Semple, T.J. MacGillivray, C. Gray, J.P. Langrish, M. Williams, M. Dweck, W. Wallace, G. McKillop, R.T. Chalmers, O.J. Garden and D.E. Newby, Abdominal aortic aneurysm growth predicted by uptake of ultrasmall superparamagnetic particles of iron oxide: A pilot study, Circulation, *Cardiovascular Imaging* **4** (2011), 274–281.
[24] J.M. Richards, C.A. Shaw, N.N. Lang, M.C. Williams, S.I. Semple, T.J. MacGillivray, C. Gray, J.H. Crawford, S.R. Alam, A.P. Atkinson, E.K. Forrest, C. Bienek, N.L. Mills, A. Burdess, K. Dhaliwal, A.J. Simpson, W.A. Wallace, A.T. Hill, P.H. Roddie, G. McKillop, T.A. Connolly, G.Z. Feuerstein, G.R. Barclay, M.L. Turner and D.E. Newby, *In vivo* mononuclear cell tracking using superparamagnetic particles of iron oxide: Feasibility and safety in humans, Circulation, *Cardiovascular Imaging* **5** (2012), 509–517.
[25] U. Sadat, S.P. Howarth, A. Usman, T.Y. Tang, M.J. Graves and J.H. Gillard, Sequential Imaging of Asymptomatic Carotid Atheroma Using Ultrasmall Superparamagnetic Iron Oxide-enhanced Magnetic Resonance Imaging: A Feasibility Study, *Journal of Stroke and Cerebrovascular Diseases: The Official Journal of National Stroke Association* **22** (2013), e271–e276.
[26] A. Saleh, M. Schroeter, C. Jonkmanns, H.P. Hartung, U. Modder and S. Jander, *In vivo* MRI of brain inflammation in human ischaemic stroke, *Brain: A Journal of Neurology* **127** (2004), 1670–1677.
[27] A. Saleh, M. Schroeter, A. Ringelstein, H.P. Hartung, M. Siebler, U. Modder and S. Jander, Iron oxide particle-enhanced MRI suggests variability of brain inflammation at early stages after ischemic stroke, *Stroke; a Journal of Cerebral Circulation* **38** (2007), 2733–2737.
[28] A. Sharma, S.V. Madhunapantula and G.P. Robertson, Toxicological considerations when creating nanoparticle-based drugs and drug delivery systems, *Expert Opin Drug Met* **8** (2012), 47–69.
[29] T.Y. Tang, S.P. Howarth, S.R. Miller, M.J. Graves, A.J. Patterson, UK-I, J.M., Z.Y. Li, S.R. Walsh, A.P. Brown, P.J. Kirkpatrick, E.A. Warburton, P.D. Hayes, K. Varty, J.R. Boyle, M.E. Gaunt, A. Zalewski and J.H. Gillard, The

ATHEROMA (Atorvastatin Therapy: Effects on Reduction of Macrophage Activity) Study. Evaluation using ultrasmall superparamagnetic iron oxide-enhanced magnetic resonance imaging in carotid disease, *Journal of the American College of Cardiology* **53** (2009), 2039–2050.

[30] T.Y. Tang, S.P. Howarth, S.R. Miller, M.J. Graves, U.K.-I. JM, Z.Y. Li, S.R. Walsh, P.D. Hayes, K. Varty and J.H. Gillard, Comparison of the inflammatory burden of truly asymptomatic carotid atheroma with atherosclerotic plaques in patients with asymptomatic carotid stenosis undergoing coronary artery bypass grafting: An ultrasmall superparamagnetic iron oxide enhanced magnetic resonance study, *European Journal of Vascular and Endovascular Surgery: The Official Journal of the European Society for Vascular Surgery* **35** (2008), 392–398.

[31] T.Y. Tang, S.P. Howarth, S.R. Miller, M.J. Graves, UK-I, J.M., R.A. Trivedi, Z.Y. Li, S.R. Walsh, A.P. Brown, P.J. Kirkpatrick, M.E. Gaunt and J.H. Gillard, Comparison of the inflammatory burden of truly asymptomatic carotid atheroma with atherosclerotic plaques contralateral to symptomatic carotid stenosis: An ultra small superparamagnetic iron oxide enhanced magnetic resonance study, *Journal of Neurology, Neurosurgery, and Psychiatry* **78** (2007), 1337–1343.

[32] T.Y. Tang, K.H. Muller, M.J. Graves, Z.Y. Li, S.R. Walsh, V. Young, U. Sadat, S.P. Howarth and J.H. Gillard, Iron oxide particles for atheroma imaging, *Arteriosclerosis, Thrombosis, and Vascular Biology* **29** (2009), 1001–1008.

[33] V.I. Teusch, W.A. Wohlgemuth, A.P. Piehler and E.M. Jung, Color-coded perfusion analysis of CEUS for pre-interventional diagnosis of microvascularisation in cases of vascular malformations, *Clin Hemorheol Micro* **58** (2014), 183–193.

[34] R. Tietze, S. Lyer, S. Durr, T. Struffert, T. Engelhorn, M. Schwarz, E. Eckert, T. Goen, S. Vasylyev, W. Peukert, F. Wiekhorst, L. Trahms, A. Dorfler and C. Alexiou, Efficient drug-delivery using magnetic nanoparticles–biodistribution and therapeutic effects in tumour bearing rabbits, *Nanomedicine: Nanotechnology, Biology, and Medicine* **9** (2013), 961–971.

[35] R.A. Trivedi, C. Mallawarachi, UK-I, J.M., M.J. Graves, J. Horsley, M.J. Goddard, A. Brown, L. Wang, P.J. Kirkpatrick, J. Brown and J.H. Gillard, Identifying inflamed carotid plaques using *in vivo* USPIO-enhanced MR imaging to label plaque macrophages, *Arteriosclerosis, Thrombosis, and Vascular Biology* **26** (2006), 1601–1606.

[36] R.A. Trivedi, U.K.-I. JM, M.J. Graves, J.J. Cross, J. Horsley, M.J. Goddard, J.N. Skepper, G. Quartey, E. Warburton, I. Joubert, L. Wang, P.J. Kirkpatrick, J. Brown and J.H. Gillard, *In vivo* detection of macrophages in human carotid atheroma: Temporal dependence of ultrasmall superparamagnetic particles of iron oxide-enhanced MRI, *Stroke; a Journal of Cerebral Circulation* **35** (2004), 1631–1635.

[37] H. Unterweger, R. Tietze, C. Janko, J. Zaloga, S. Lyer, S. Durr, N. Taccardi, O.M. Goudouri, A. Hoppe, D. Eberbeck, D.W. Schubert, A.R. Boccaccini and C. Alexiou, Development and characterization of magnetic iron oxide nanoparticles with a cisplatin-bearing polymer coating for targeted drug delivery, *International Journal of Nanomedicine* **9** (2014), 3659–3676.

[38] S. Wahajuddin, Arora, Superparamagnetic iron oxide nanoparticles: Magnetic nanoplatforms as drug carriers, *International Journal of Nanomedicine* **7** (2012), 3445–3471.

[39] J.L. Winer, C.Y. Liu and M.L. Apuzzo, The use of nanoparticles as contrast media in neuroimaging: A statement on toxicity, *World Neurosurgery* **78** (2012), 709–711.

[40] A. Yilmaz, M.A. Dengler, H. van der Kuip, H. Yildiz, S. Rosch, S. Klumpp, K. Klingel, R. Kandolf, X. Helluy, K.H. Hiller, P.M. Jakob and U. Sechtem, Imaging of myocardial infarction using ultrasmall superparamagnetic iron oxide nanoparticles: A human study using a multi-parametric cardiovascular magnetic resonance imaging approach, *European Heart Journal* **34** (2013), 462–475.

[41] A. Yilmaz, S. Rosch, K. Klingel, R. Kandolf, X. Helluy, K.H. Hiller, P.M. Jakob and U. Sechtem, Magnetic resonance imaging (MRI) of inflamed myocardium using iron oxide nanoparticles in patients with acute myocardial infarction - preliminary results, *International Journal of Cardiology* **163** (2013), 175–182.

[42] J. Zaloga, C. Janko, J. Nowak, J. Matuszak, S. Knaup, D. Eberbeck, R. Tietze, H. Unterweger, R.P. Friedrich, S. Duerr, R. Heimke-Brinck, E. Baum, I. Cicha, F. Dorje, S. Odenbach, S. Lyer, G. Lee and C. Alexiou, Development of a lauric acid/albumin hybrid iron oxide nanoparticle system with improved biocompatibility, *International Journal of Nanomedicine* **9** (2014), 4847–4866.

[43] W.J. Zhang and B. Frei, Albumin selectively inhibits TNF alpha-induced expression of vascular cell adhesion molecule-1 in human aortic endothelial cells, *Cardiovasc Res* **55** (2002), 820–829.

[44] Y. Zhang, W. Li, L. Ou, W. Wang, E. Delyagina, C. Lux, H. Sorg, K. Riehemann, G. Steinhoff and N. Ma, Targeted delivery of human VEGF gene via complexes of magnetic nanoparticle-adenoviral vectors enhanced cardiac regeneration, *PloS One* **7** (2012), e39490.

[45] S.G. Zheng, H.X. Xu, L.N. Liu, Y. Wang, Y.F. Zhang, L.H. Guo, C. Liu, J.M. Xu, L.P. Sun and J. Wu, Parametric imaging with contrast-enhanced ultrasound: Usefulness for characterization of dynamic effects of microvascularization for hepatocellular carcinoma and focal nodular hyperplasia, *Clin Hemorheol Micro* **55** (2013), 375–389.

Supplementary material

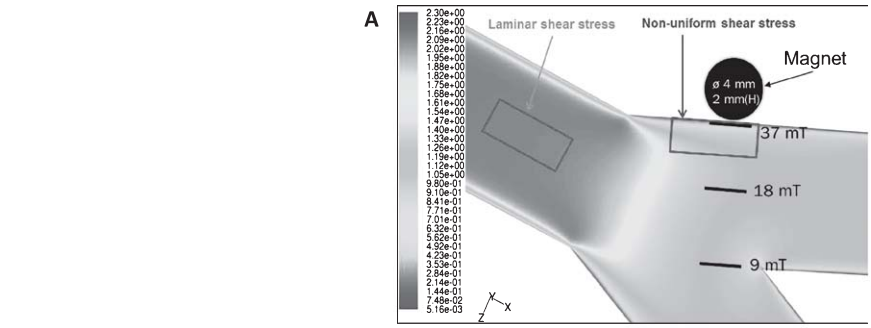

	SPION-1	SPION-2	SPION-3
Hydrodynamic diameter [nm]	126	79	78
Zeta-potential [mV]	-34.6	-37.3	+0.1

Supplementary Fig. 1. Schematic presentation of bifurcating slide with magnet placement(A) and physico-chemical characterization of SPIONs (B). (A) Wall shear stress pattern in bifurcating slides, color scale in Pa (1Pa = 10 dyne/cm^2), regions of laminar or non-uniform shear stress are indicated. Schematic presentation of magnet placement for the targeted accumulation of nanoparticles and the magnetic flux density measured with a teslameter are shown. (B) TEM images and physicochemical characterization of SPIONs.

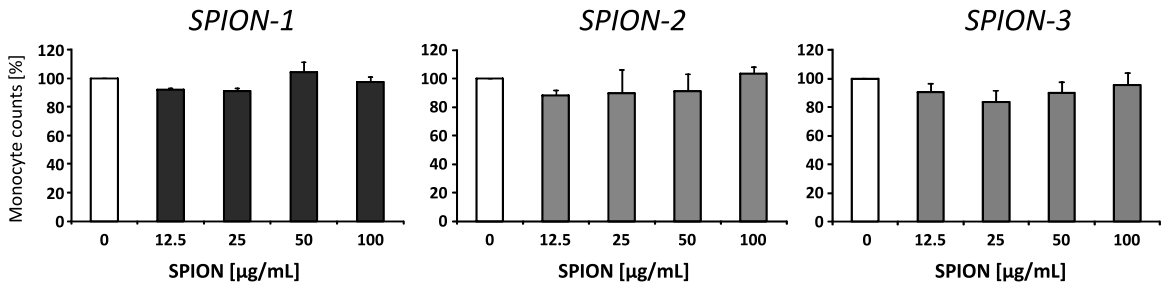

Supplementary Fig. 2. Viability of THP-1 monocytic cells. THP-1 cells pre-incubated with SPIONs (2 h at indicated concentrations) were counted with flow cytometry. Untreated control samples were set to 100%. Data are expressed as mean ± SEM; n = 3.

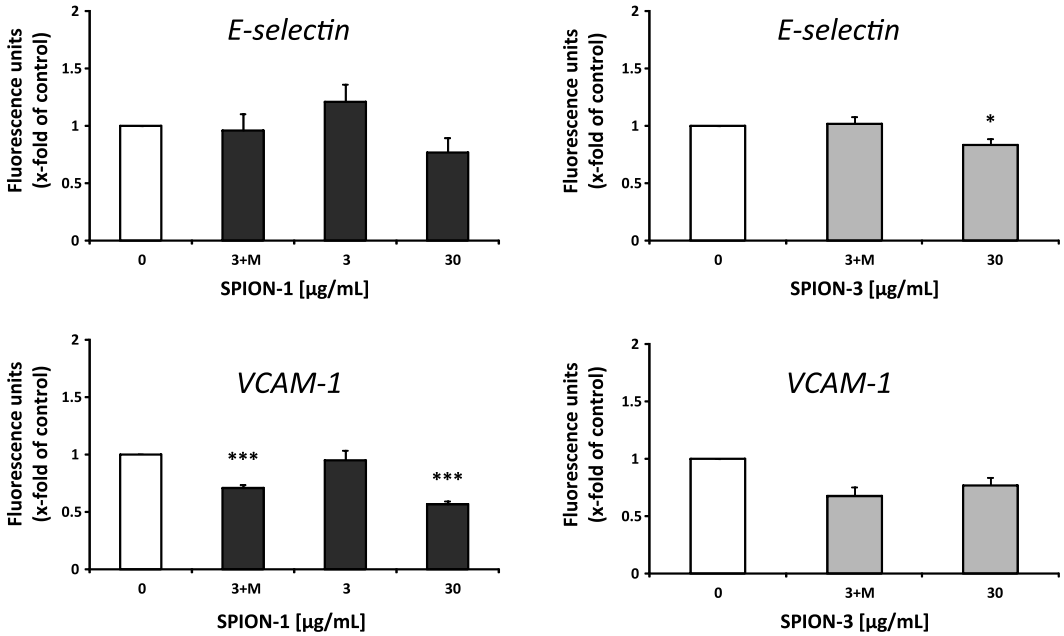

Supplementary Fig. 3. Adhesion molecule expression. HUVECs were perfused with SPION-1(red) and SPION-3 (green) for 18 h in bifurcation flow-through slides. SPION concentrations are indicated; 3+M denotes the branch with magnet and 3 the branch without magnet. Cells were stimulated with TNF-α (2h) and stained with primary antibody against E-selection or VCAM-1. Fluorescence was quantified in 6–8 microscopic images per experiment (non-uniform region, 20x objective magnification).Values obtained in untreated control samples were set to 1. Data are expressed as mean ± SEM; n = 3. $^{*}p < 0.05$; $^{**}p < 0.01$; $^{***}p < 0.001$ vs. control. Signed Rank test of paired Student's T-test.